Defect acceptability under full-scale fretting fatigue tests for railway axles

S. Foletti [a,*], S. Beretta [a], G. Gurer [b]

[a] Politecnico di Milano, Dipartimento di Meccanica, Via La Masa 1, 20156 Milan, Italy
[b] Middle East Technical University, Department of Metallurgical and Materials Engineering, 06800 Ankara, Turkey

This paper presents a new approach based on the application of a multiaxial high cycle fatigue criterion together with the use of El-Haddad correction for investigation of fretting fatigue in railway axles. Stress path along the axle–wheel contact, determined by the FE analysis, was implemented into different mul-tiaxial fatigue criteria in order to predict critical sites of nucleation. The equivalent fatigue limit expressed by the applied criterion is compared with the crack size dependent fatigue limit described by El-Haddad correction in order to define a defect size acceptability criterion. Verification of the proposed approach was done by post-test failure investigation of the full-scale axle tests conducted as a part of Euraxles project. Scanning electron microscope (SEM) examination of the failed press-fit sections revealed a critical defect size in the order of 200 μm in depth for non-propagating cracks. The obtained results were found to be consistent with the estimations made by the proposed approach.

Keywords:
Fretting fatigue
Multiaxial fatigue criteria
Defect acceptability
Railway axles

1. Introduction

Investigation of fretting damage and its prolonged consequences in fatigue life assessment is an important issue in railway axle design. Fretting fatigue in the axle–wheel contact can be described as the repetitive micro sliding of the wheel assembly on press-fit seat due to applied bending and vibration. Multiple-site surface damage caused by fretting is considered to be the source of crack nucleation which can become a propagating crack with further application of cyclic loading. A decreased fatigue life up to 60–75% due to fretting damage has been reported in the lit-erature [1,2].

The present study is a part of research activity devoted to validate the fatigue limits described by the European Standards. Main objective of the present study is to develop an acceptability criteria that can be applied in assessment of surface defects inspected at axle press-fits by magnetic particle inspections (MPI). Further contribution to the European Standard EN-13260, which necessitates verification of no crack formation after 10^7 cycles at fatigue limit currently, by evaluating the applicability of presents fatigue limits in the presence of non-propagating surface cracks was also aimed [3]. In the study, press fit surfaces of different EA4T axles have been investigated. A nominal bending stress, not exceeding 240 MPa, was selected in accordance with the EN standards [4–6]. The allowable stress limit at the press fit was reduced to 132 MPa for an axle with a diameter ratio of D/d = 1.12 (Fig. 1a) [4,5]. Formation and developments of non-propagating cracks at the press-fit under the influence of fretting was investigated.

A previous study on fretting fatigue of railway axles identified four typical regions for initiation sites located at the root of transition fillet (T-transition), contact edge, stick–slip interface of the contact and sub-surface under contact [4,5]. Hirakawa et al. reported formation of an annular band of fretting corrosion with a width of 7–9 mm starting from the edge of press-fit to the inner press fitted surface for railway axles. Within this band several minute cracks can be observed. However, the cracks which propagated to final failure always observed to initiate from the sites 2–5 mm away from the edge of the press-fit [7].

Mechanism of fretting fatigue in railway axle is explained by the multiple-site nucleation of non-propagating cracks under the influence of fretting damage described as multiple-site damage (MSD) [8]. Beyond certain limits of loading, framed by application of multiaxial fatigue criteria along the stress path, transformation of non-propagating cracks to a state of propagation might take place. Propagation of long-cracks, driven by the applied bulk stress, results in final fracture of the axle as cyclic loading proceeds [8]. Experimental fretting studies on different materials has shown that majority of fatigue life has been spent in formation of a engineering crack in the cases of cylindrical contacts [1,8–13]. In other

* Corresponding author.
E-mail address: stefano.foletti@polimi.it (S. Foletti).

Published Journal Article available at: http://dx.doi.org/10.1016/j.ijfatigue.2015.08.023

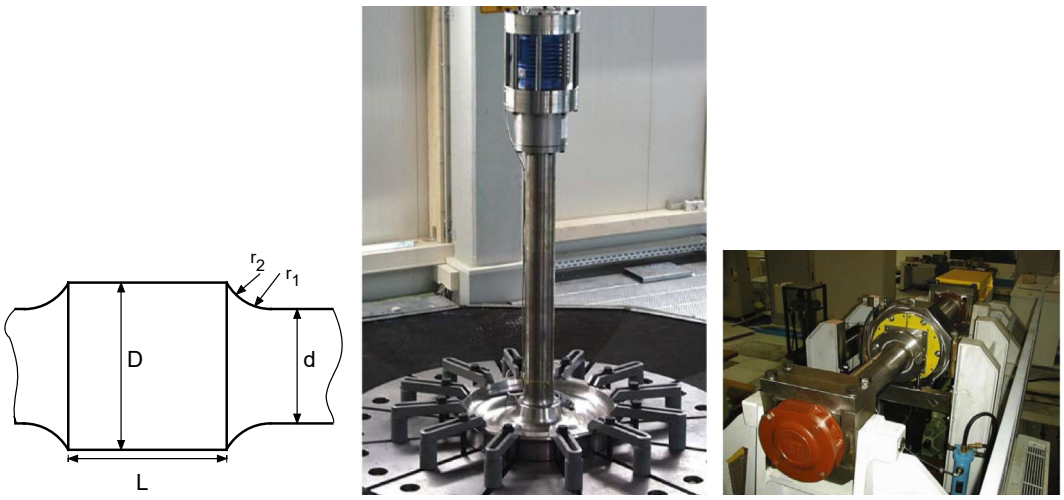

Fig. 1. Test rigs and testpiece geometry: (a) Detailed shape of the press-fitted part. (b) Test rig for Minden type tests. (c) Test rig for Vitry type tests.

words, a rapid increase in crack propagation rate is observed when the propagating cracks originated from different sources are merged with one another to form a major crack.

For the reasons given determination of the limiting size for non-propagating cracks and selection of a proper multiaxial fatigue criterion well-describing the multiaxiality of the applied load case is essential. In the present study, two different multiaxial criteria, Dang Van [14] and Liu–Mahadevan [15], were applied to the stress distribution along press-fit contact obtained by finite element (FE) analysis.These two criteria, with a suitable modification for Dang Van [16] have presented remarkable results for the investigation of microcrack advance under influence the rolling contact fatigue [17].The obtained equivalent stress for each criterion was checked against the fatigue limit of the material expressed as a function of defect size through the El Haddad correction [18].The prediction capability for the proposed approach has been evaluated by comparing full-scale axle test results, performed as a part of Euraxles project with the data produced by the analytical approach [19]. Axles with two different axle geometries were tested in test benches until a fatigue life of 10^7 cycles was achieved. Tested axles are dismantled and prepared for macro and micro examination.

In macro examination, magnetic particle inspection (MPI) of the failed and run-out axles was done in order to detect indications of macro cracking under press-fit seat region. Inspected orientations of major cracks are measured and expressed in distance with respect to the contact edge. Obtained experimental results are compared with the critical site estimations made by the proposed analytical method.

Micro examination was done on the samples sectioned from the cracked regions identified by macro examination. Sectioned samples were examined under SEM in order to investigate size,orientation and distribution of non-propagating cracks as well as the defect size from which a crack starts to propagate. Crack size measurements taken from the SEM images were used in characterization of critical size for non-propagating cracks. Obtained results are compared with the critical size estimations for the corresponding region made by the proposed analytical method. In conclusion, the applicability of each multiaxial fatigue criterion for explaining the limiting conditions for fretting fatigue of railway axles has been discussed.

Table 1
Axle geometry at press-fit.

	D [mm]	d [mm]	D/d	r_1 [mm]	r_2 [mm]	l [mm]
F1-Vitry	190	160	1.19	75	15	185
F4-Vitry	165	147	1.12	75	15	185
F4-Minden	165	147	1.12	75	15	190

Table 2
Full scale fretting fatigue test results on railway axles.

Test rig type	Test #	σ_{nom} [MPa]	Test results	Failure location – main crack
F1-Vitry	1	153	Failed ($N = 1.69 \times 10^6$ cycles)	Wheel seat at about 20 mm from the T-transition
F1-Vitry	2	141	Run-out ($N = 10^7$ cycles)	
F1-Vitry	3	153	Failed ($N = 1.47 \times 10^6$ cycles)	Wheel seat at about 20 mm from the T-transition
F4-Vitry	1	120	Failed ($N = 7.70\text{x}10^6$ cycles)	Wheel seat at about 10 mm from the T-transition
F4-Vitry	2	108	Run-out ($N = 10^7$ cycles)	
F4-Vitry	3	120	Run-out ($N = 10^7$ cycles)	
F4-Vitry	4	132	Failed ($N = 4.98 \times 10^6$ cycles)	Wheel seat at about 10 mm from the T-transition
F4-Vitry	5	120	Failed ($N = 2.10 \times 10^6$ cycles)	Wheel seat at about 10 mm from the T-transition
F4-Minden	1	132	Failed ($N = 10^7$ cycles)	Wheel seat at about 4 mm from the T-transition
F4-Minden	2	126	Failed ($N = 10^7$ cycles)	Wheel seat at about 15 mm from the T-transition
F4-Minden	3	120	Run-Out ($N = 10^7$ cycles)	
F4-Minden	4	132	Failed ($N = 10^7$ cycles)	Wheel seat at about 7 mm from the T-transition

2. The proposed method

The procedure is based on a finite element (FE) analysis so as to obtain the stress path under the press fit seat. The stress tensor is used as input in a multiaxial high cycle fatigue (HCF) criterion to determine an equivalent stress:

$$\sigma_{eq} = f(\text{HCF criterion}, [\sigma_{ij}], X, Y) \tag{1}$$

as a function f of the selected multiaxial HCF criterion and the stress tensor $[\sigma_{ij}]$ at a specific location in the press fit seat identified by the coordinates X and Y.

The so obtained equivalent stress is checked against the fatigue limit of the material expressed as a function of defect size through the El-Haddad correction, [18]:

$$\sigma_w = \sigma_{w0}\sqrt{\frac{\sqrt{\text{area}_0}}{\sqrt{\text{area}} + \sqrt{\text{area}_0}}} \tag{2}$$

being σ_{w0} the fatigue limit for smooth specimens, σ_w the fatigue limit depending on defect size (expressed in terms of Murakami's $\sqrt{\text{area}}$ parameter [20]) and the fictitious crack length parameter ($\sqrt{\text{area}_0}$) found by interpolating the fatigue limit experimentally obtained for different defect sizes.

In the case of no crack formation, that is when the $\sqrt{\text{area}}$ term is zero, equivalent stress level equals to the material fatigue limit for smooth specimen. Beyond this limit a fatigue crack would initiate and propagate spontaneously. For the cases of stress application lower than material fatigue limit a prospective defect size along the damaged area can be defined. That is, a reduced equivalent stress can be described by Eq. (3).

$$\sigma_{eq} = \sigma_w \Rightarrow \sqrt{\text{area}} = \left(\left(\frac{\sigma_{w0}}{\sigma_{eq}}\right)^2 - 1\right)\sqrt{\text{area}_0} \tag{3}$$

Finally, to obtain the crack size of a shallow 2D surface crack it is possible to use the relationship presented in Eq. (4) [20]:

$$\sqrt{\text{area}} = \sqrt{10}c \tag{4}$$

where c is the crack depth of the inclined crack length along the critical plane predicted by the multiaxial fatigue criteria (Fig. 5b).

2.1. Multiaxial high cycle fatigue criteria

Two different multiaxial high cycle fatigue criteria (the Dang Van criterion and the Liu–Mahadevan criterion) have been used in the proposed procedure. In literature, applicability of the selected criteria have been discussed several times for the analytical solution of rolling contact and fretting type of fatigue failures [9,21,22].

2.1.1. Modified Dang Van fatigue criterion

The basis of the Dang Van criterion is the application of the elastic shakedown principles at the mesoscopic scale (more details can be found in Refs. [14,23]). The Dang Van criterion can be expressed by:

$$\tau_{DV}(t) + \alpha_{DV}\sigma_h(t) \leqslant \tau_w \tag{5}$$

where α_{DV} is a material constant, τ_w is the fatigue limit in reversed torsion, $\sigma_h(t)$ is the instantaneous hydrostatic component of the

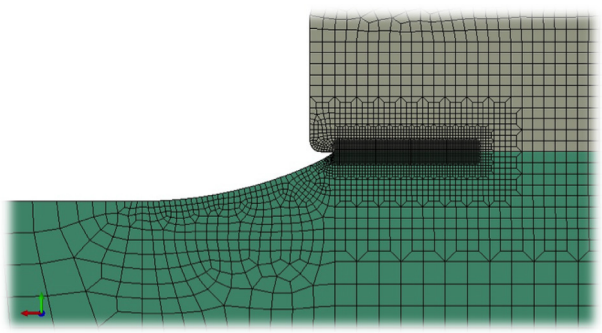

Fig. 3. Finite element mesh in the press fit seat.

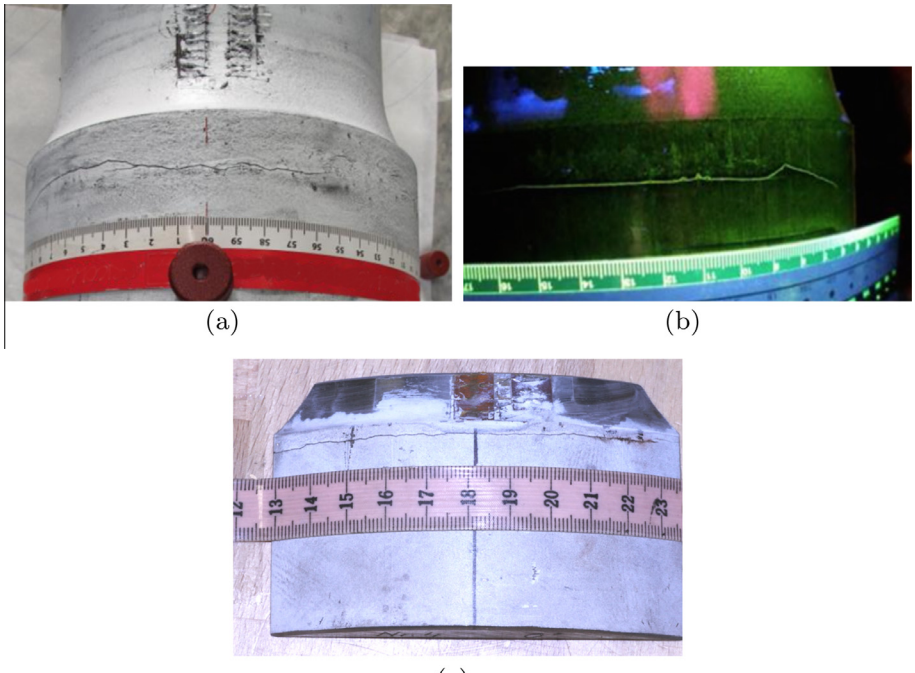

Fig. 2. Failure location: (a) F1 axle tested on Vitry test rig, (b) F4 axle tested on Vitry test rig, (c) F4 axle tested on Minden test rig.

stress tensor and $\tau_{DV}(t)$ is the instantaneous value of the Tresca shear stress expressed by Eq. (6):

$$\tau_{DV}(t) = \frac{\hat{s}_I(t) - \hat{s}_{III}(t)}{2} \tag{6}$$

evaluated over a symmetrized stress deviator found at the mesoscopic scale, which is obtained by subtracting from the deviatoric stress $s_{ij}(t)$ a constant tensor, $s_{ij,m}$:

$$\hat{s}_{ij}(t) = s_{ij}(t) - s_{ij,m} \tag{7}$$

where $s_{ij,m}$ is a residual stress deviator, fulfilling the condition of an elastic shakedown state at the mesoscopic scale.

The constant α_{DV} appearing in the expression of the Dang Van criterion is usually related with the tension–compression fatigue limit σ_w and the pure torsion fatigue limit, τ_w:

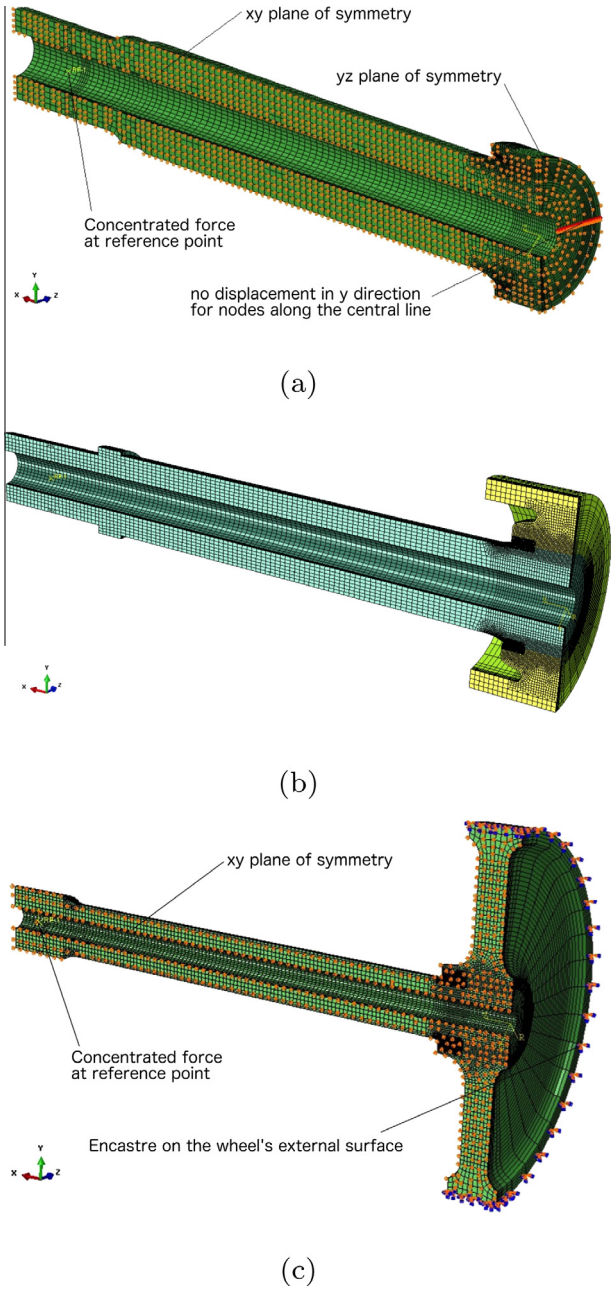

Fig. 4. Finite element model: (a) F1 axle tested on Vitry test rig, (b) F4 axle tested on Vitry test rig, (c) F4 axle tested on Minden test rig.

$$\alpha_{DV} = 3\left(\frac{\tau_w}{\sigma_w} - \frac{1}{2}\right) \tag{8}$$

The resulting failure locus presented by a line on τ_{DV}—σ_h plane. In order to avoid non-conservative prediction in rolling contact fatigue problem, Desimone et al. [16], argued that the failure locus in the region with $\sigma_h < 0$ should be modified into a constant value $\tau_w = 0.5\sigma_w$ (proposed conservative locus):

$$\tau_{DV}(t) \leqslant \tau_w = \frac{\sigma_w}{2} \text{ if } \sigma_h < 0 \tag{9}$$

Further analyses and experimental fatigue tests on mild railway wheel steel subjected to out-of-phase multiaxial fatigue loading, simulating rolling contact fatigue conditions, have shown that the multiaxial fatigue limit does not depend on hydrostatic stress if the hydrostatic stress component is lower than zero [17]. Further-more, non-conservative results were achieved by the application of the original locus concept. For this reason, the Dang–Van criterion will be applied in "modified" form in the present study. In fact, the stress analysis of the region under examination reveals the hydrostatic stress to remain negative during process of loading. The Dang Van criterion, in its modified forms, will be applied in the present study. Using the proposed failure locus the fatigue limit condition for $\sigma_h <$ 0 simply becomes:

$$\sigma_{eq}^{DV} = 2\max\left(\tau_{DV}(t)\right) \leqslant \sigma_w \tag{10}$$

As already pointed out a prospective non-propagating crack, as well as a defect, is described both by its length and orientation. The previously described Dang Van model is able to predict the length but does not present any information about the orientation. For this reason, a critical plane based version of the Dang Van criterion

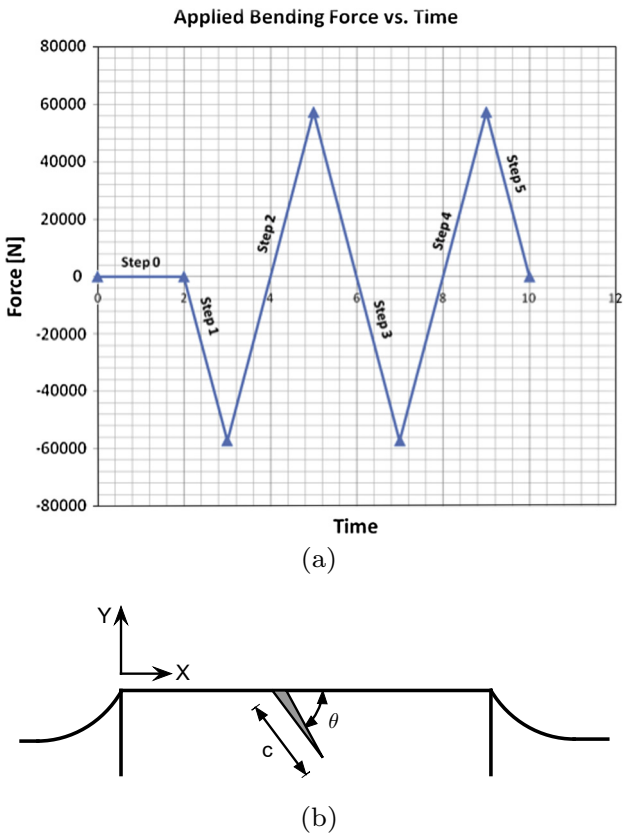

Fig. 5. (a) Load step in finite element analysis, (b) local reference system.

was used in the study. When compared to the basic Dang Van relation a negligible difference in terms of equivalent stress is expected.

Considering a material plane defined by its unit normal vector $\underline{n}$ the Dang Van shear stress can be defined as expressed in Eq. (11):

$$\tau_{DV}(\phi,\theta,t) = ||\underline{\tau}(\phi,\theta,t) - \underline{\tau}_m(\phi,\theta)|| \tag{11}$$

where ϕ, θ are the spherical angles used to express the unit normal vector $\underline{n}$ in a O_{xyz} frame. $\underline{\tau}(\phi,\theta,t)$ is the shear stress vector acting on the material plane under consideration, $\underline{\tau}_m(\phi,\theta)$ is the mean shear stress vector and the bracket symbol ($\|\ \|$) represents the length (measure) of the enclosed vector.

Computing the mean shear stress $\underline{\tau}_m(\phi,\theta)$ on every plane passing through a point of the body, the determination of the critical plane according to Dang Van criterion requires the solution of the double maximization problem presented in Eq. (12).

$$\max_{\phi,\theta}\left[\max_{t}\|\underline{\tau}(\phi,\theta,t) - \underline{\tau}_m(\phi,\theta)\|\right] \tag{12}$$

2.1.2. Liu–Mahadevan fatigue criterion

The Liu–Mahadevan criterion [15,24] is a high cycle fatigue criterion based on the definition of a critical plane and a fatigue fracture plane. The fracture plane is the crack plane observed at macro level, while the critical plane is a material plane where the fatigue damage is evaluated. In the original proposed model the fracture

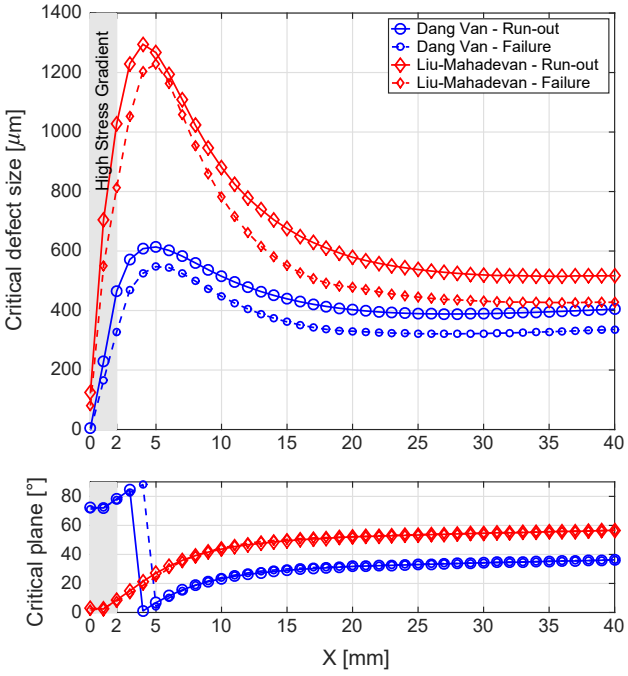

Fig. 7. Surface critical defect size and critical plane for F1 axle.

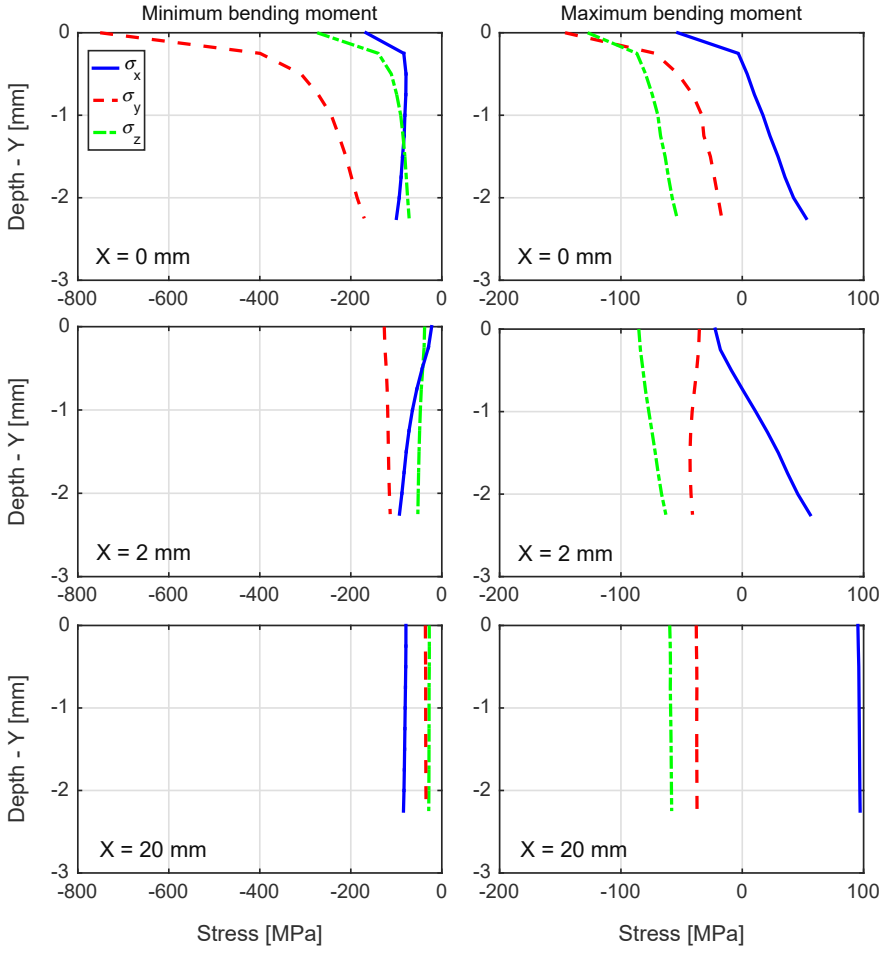

Fig. 6. Stress gradient along the contact.

plane is defined as the plane which experiences the maximum normal stress amplitude. The critical plane orientation may differ from the fatigue fracture plane for different materials [15]. In the general case the angle α, between the fracture and the critical plane, can be obtained as a function of the ratio $s = \tau_w/\sigma_w$ between the torsional and the uniaxial fully reversed fatigue limit:

$$\cos(2\alpha) = \frac{-2 + \sqrt{4 - 4(1/s^2 - 3)(5 - 1/s^2 - 4s^2)}}{2(5 - 1/s^2 - 4s^2)} \tag{13}$$

Once the critical plane has been defined, the fatigue model is expressed by Eq. (14):

$$\sigma_{eq} = \frac{1}{\beta}\sqrt{\left[\sigma_{a,c}\left(1 + \eta\frac{\sigma_{m,c}}{\sigma_w}\right)\right]^2 + \frac{1}{s^2}(\tau_{a,c})^2 + k\left(\sigma^H_{a,c}\right)^2} \tag{14}$$

where $\sigma_{a,c}$, $\tau_{a,c}$ and $\sigma^H_{a,c}$ are the normal stress amplitude, shear stress amplitude and hydrostatic stress amplitude acting on the critical plane respectively. $\sigma_{m,c}$ is the mean normal stress acting on the critical plane. β, η, and k are material parameters depending on the ratio s. For ductile materials:

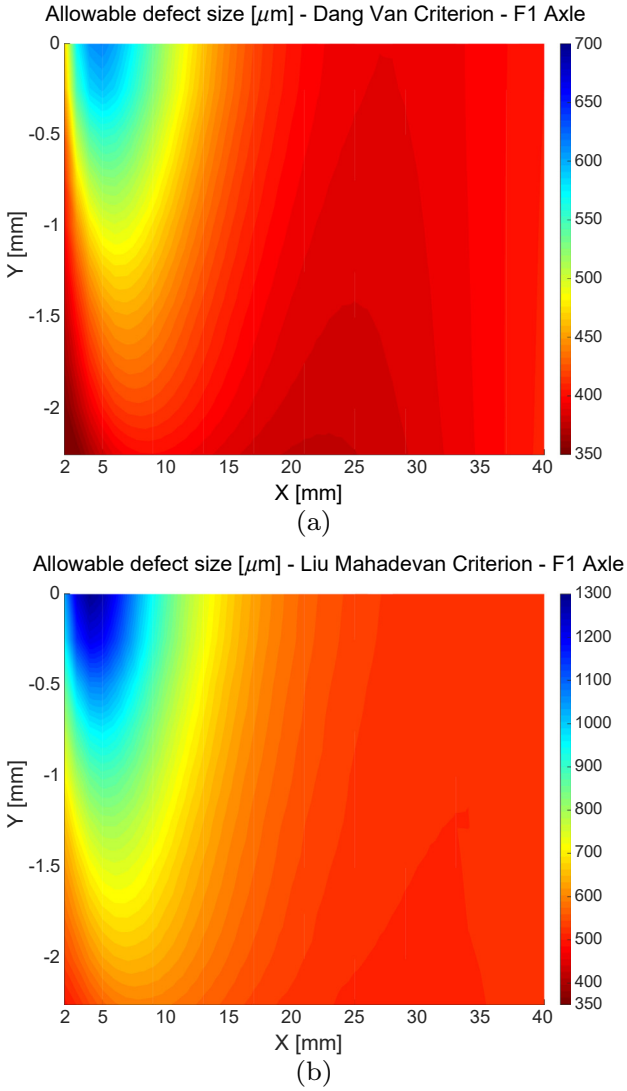

Fig. 8. Sub-surface critical defect size for F1 axle under run-out condition: (a) Dang van criterion, (b) Liu–Mahadevan criterion.

$$s = \frac{\tau_w}{\sigma_w} < 1 \Rightarrow \begin{cases} \beta = \sqrt{\cos^2(2\alpha)s^2 + \sin^2(2\alpha)} \\ k = 0 \\ \eta = \frac{3}{4} + \frac{1}{4}\left(\frac{\sqrt{3}-1/s}{\sqrt{3}-1}\right) \end{cases} \tag{15}$$

3. Comparison with experimental results

The prediction capability of the proposed method has been checked with respect to the experimental results of fretting fatigue tests conducted on full scale EA4T railway axles [19]. The fatigue tests were carried out as a part of Euraxles project. In the project fatigue testing of different axle geometries by Vitry and Minden types of test rigs was carried out (Fig. 1b and c). The so called Minden type test rig is a cantilever resonant machine where the axle is constrained with a rigid wheel adaptor on one side and an electric motor with rotating unbalanced masses fixed on the opposite side (Fig. 1b). The so called Vitry type test rig is a three point rotating bending device where the axle, rotated by a motor, is simply supported by two journal axle bearing boxes and loaded in the middle by an actuator (Fig. 1c).

Two axle geometries, F1 Geometry tested by Politecnico di Milano on a Vitry type test rig and F4 Geometry tested both on a Minden (by DB – Deutsche Bahn) and Vitry (by SNCF – National society of French railways) type test rig, will be considered in present paper. Here D and d are the maximum and minimum diameters at the transition of press-fit, see Fig. 1a. The dimensional details of the tested axles are reported in Table 1. The F1 geometry was designed to obtain the axle body fatigue limit of free surfaces without press fits as described by the European Standard EN-13261 [6].

On the contrary, the F4 geometry has been designed to evaluate the fatigue limit at press-fit. The selected diameter ratio $D/d = 1.12$ is the minimum accepted value in the design of axles that may be reached in service due to some consecutive seat re-profiling made in maintenance [6].

The F4 axles tested both on Minden or Vitry test rig are identical in terms of diameter of the seat (D), diameter of the body (d), the corresponding diameter ratio (D/d) and the shape of the transition (radius and length). There are differences in the dummy hub press fitted on the axle to recreate the normal wheelset condition. More details about test rigs and axles geometry can be found in Ref. [19].

Considering the unexpected fretting failures at press fit the verification of the proposed method was processed with the data acquired from F1 and F4 axles. Results obtained from fatigue testing and corresponding macro examination are presented in Table 2 for different values of applied nominal bending stresses computed at the maximum axle diameter. Location and distribution of cracks, detected by magnetic particle inspections, made on broken axles of types F1 and F4, are shown in Fig. 2.

The proposed method has been applied to the results obtained by the FEA analysis of the press fit. Both of the multiaxial fatigue criteria were applied on the acquired stress state separately. The ratio s between the torsional and the axial fatigue limit, which is typically $s = \tau_w/\sigma_w = 0.85$ for materials containing defects, was kept constant independent of the defect size for the Liu–Mahadevan criterion [25]. The fatigue properties of EA4T steel have been taken from Refs. [26,27], where a series of fatigue tests in presence of microdefects were carried for determining σ_{w0} and $\sqrt{\text{area}_0}$ (see Eq. (2)).

3.1. Finite element model

Several FE analyses have been carried out to simulate experimental tests to obtain the stress path in the critical regions of the shaft [28]. 3D FE model has been obtained by the revolution

of a 2D solid mesh in order to obtain regular distribution of solid elements. The starting 2D solid mesh was built by adapting Abaqus rectangular elements CAX4R. An element size of 0.25 × 0.25 mm was selected in the area of interest which is the volume including the press fit seat and sub-surface associated with it (Fig. 3). Linear type of elements, convergence of which has been found to be similar to that of parabolic elements for the given size as presented by an earlier report published by the project, were selected [29]. The obtained 3D model is composed of Abaqus C3D8R elements (8-node linear brick) with reduced integration and hourglass control.

The interaction between shaft and wheel is modeled with a standard surface to surface contact. Tangential behavior is described with a linear friction coefficient equal to 0.6 as it was experimentally evaluated in the Euraxles project starting from the press fitting diagram and from the strain measurements along the transition. The interference fit was introduced in the first step with the use of maximum value supplied by technical drawings (0.313 mm for F1 axle and 0.277 mm for F4 axle). The bending load was applied to a reference node, linked to the interested section by a coupling-joint. In Fig. 4a the boundary conditions used in the Vitry type test for F1 axle are presented. *X* axis displacements were not allowed on *xy* symmetry plane and only radial displacements were allowed on *yz* symmetry plane. Additionally, displacement along y direction was not allowed for the nodes along central line in order to achieve an isostatic condition. The finite element model for F4 geometry tested on the Vitry test rig is reported in Fig. 4b. The boundary conditions are the same as previously pointed out. For Minden type test, *xy* plane symmetry was imposed only. Exter-nal surface of the wheel has been fastened (Fig. 4c). Two different analyses with different applied nominal stresses levels, selected on the basis of "failure" and "run-out" stress levels observed in full-scale tests, presented in Table 2, were conducted for each type of axle.

The stress data after two complete cycles of load application was considered in order to obtain stress state after a stabilized condition have been attained (Fig. 5a). On a *X*-*Y* reference plane, origin of which is selected at the contact edge with an *X* axis parallel to the longitudinal axis of the axle and a *Y* axis in the radial direction, stress path from the last cycle was extracted (Fig. 5b). Cyclic stress at each node has been expressed by the mean stress tensor and amplitude stress tensor with respect to the defined coordinate system.

3.2. F1 axle

The stress profile at distances 0, 2 and 20 mm away from the contact edge is shown in Fig. 6. A steep stress gradient is observed near T transition. Together with the mesh diagram presented in Fig. 3, computation of a mesh size dependent stress singularity is obviously seen. In order to achieve proper results application of proposed "local stress based" high cycle fatigue criteria to the singularity region was avoided. For the assessment of the imposed limitation surface examination of the tested axles was made. MP inspection showed the distribution of the fretting fatigue initiation sites to range between 4 mm and 20 mm away from contact edge. Obtained results were also justified by the study presented in [7]. Accordingly, the proposed method was applied to the regions of reduced stress gradient starting from 2 mm away from the transition edge ($X \geqslant 2$ mm). The presented approach could be extended

Table 3
Predicted allowable defect size (length) *c*. Subscripts: (DV) Dang Van Criterion, (LM) Liu–Mahadevan Criterion, (*exp*, *CP*) experimentally observed defect size (length) with crack propagation, (*exp*, *NCP*) experimentally observed defect size (length) with no crack propagation, (–) no SEM observations.

	σ_{nom} [MPa]	c_{DV} [μm]	c_{LM} [μm]	$c_{exp,CP}$ [μm]	$c_{exp,NCP}$ [μm]
F1 failure	153	320	420	> 360	<185
F1 run-out	141	390	520	–	–
F4 failure	132	450	430	–	–
F4 run-out	120	540	510	–	<120

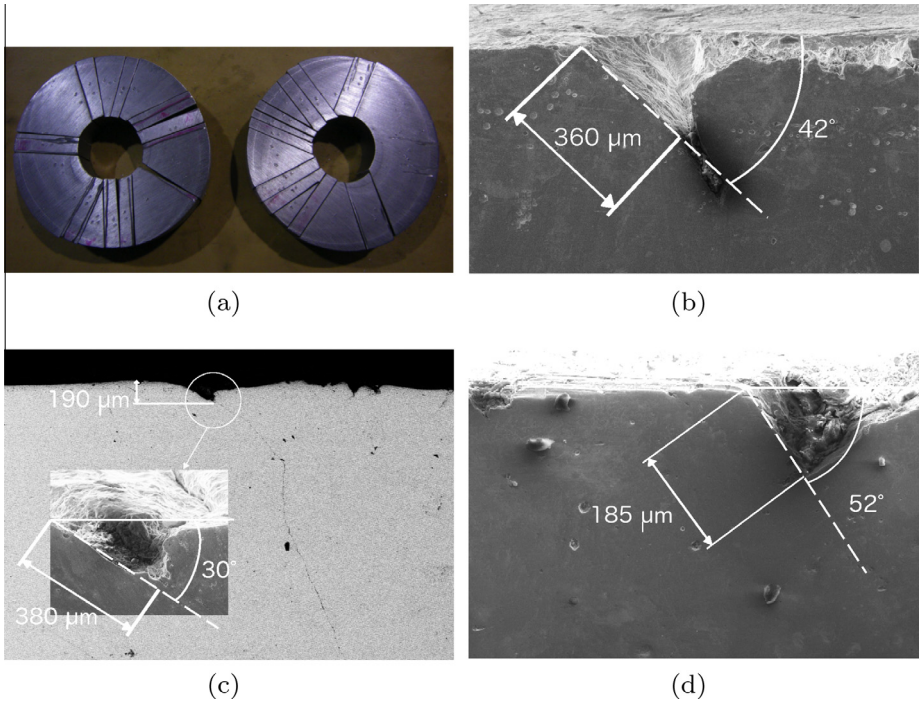

Fig. 9. Fractographic analysis for F1 axle tested at failure condition: (a) Axle's sectioning, (b and c) cavitation and cracking on tangential direction leading to crack propagation, (d) surface defects with non-propagating cracks.

to the vicinity of contact edge by applying a criterion without local stress variables [10,30].

The estimations of non-propagating crack size and critical plane orientation are shown in Fig. 7 for the state of stress at the surface, ($Y = 0$). In this region for both criteria the most sensitive region for crack propagation was predicted to be between 20 and 30 mm from transition edge, in full agreement with experimentally observed failure location, (Fig. 2a). At the failure stress level the critical defect size at the onset of crack propagation predicted by the criteria is in the order of 300–400 μm where the smaller value is the limit predicted by the Dang Van criterion. For the run-out axles the critical defect size increase to 390 μm and 520 μm by Dang Van criterion and Liu Mahadevan criterion, respectively.

From the critical plane analysis the corresponding critical plane angles are found to be $\theta = 33^\circ$ for Dang Van criterion and $\theta = 53^\circ$ for the Liu–Mahadevan criterion. (Fig. 7). Evaluation of the critical planes at different stress levels has also shown the independence of the critical planes from the applied nominal stress.

Comprehensive analysis of the sub-surface region under the press-fit was made. Subsurface analysis reveals a slight decrease in allowable defect size and, thus increased sensitivity to crack propagation (Fig. 8).The main difference between the two criteria is in terms of allowable defect size predicted near the T-transition. The Liu–Mahadevan criterion gives non-conservative results, with a critical defect greater than 700 μm, close to the T-transition when compared to the estimations made by DangVan criterion.

In order to decide about applicability and prediction ability of the applied HCF criteria, investigation of surface defects present along contact surface close to the observed cracks was done.

A visual inspection has been performed on the axle broken at 153 MPa (axle nr.1 in Table 2) for determination of crack shape, dimension and location. The analysis was focused on both sides of the T transition where the visible cracks were observed. The inspection revealed the presence of a major crack through the whole thickness, at about 20 mm from the border. Moreover, a lot of smaller evident cracks located at a distance about 10 mm away from the contact edges at the both sides of the transition are observed (Fig. 2a).

According to the results presented in Fig. 7 location of initiation sites are successfully predicted by the applied criteria. A comprehensive SEM analysis has been performed on the specimens sectioned from the critical regions in order to investigate depth, propagation path and origin of the cracks as well as the severity of the fretting damage on material surface (Fig. 9a). Propagating cracks originated from surface defects were observed in many cases (Fig. 9b and c). The typical size of the defect from which a propagating crack is nucleated is in the order of 350–400 μm in length which is consistent with the value predicted by both of the criteria. In Fig. 9d a section of press-fit including non-propagating cracks with dimensions in the order of 200 μm in size is shown. The angles of propagation are measured to be 30° and 40° from the images presented in Fig. 9c and b, respectively which are comparable to the estimations made by the Dang–Van criterion.

Results of the experimental measurements and predictions of permissible defect sizes are tabulated in Table 3.

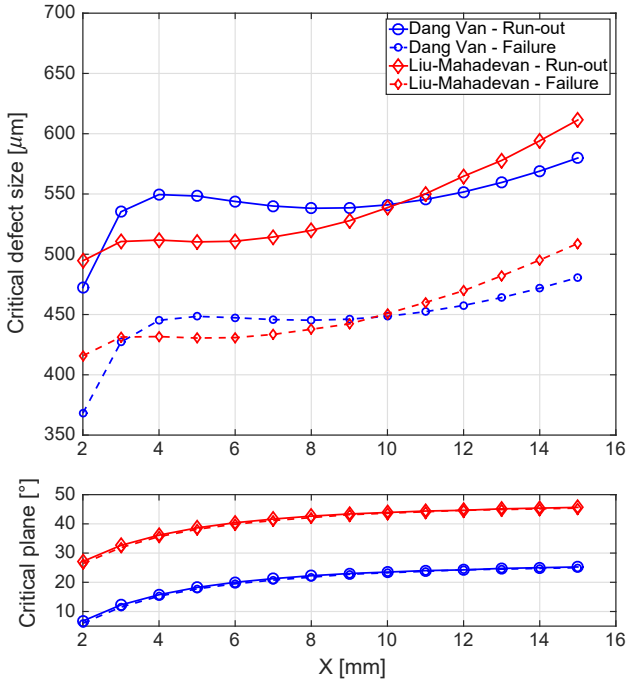

Fig. 10. Surface critical defect size and critical plane for F4 axle – Minden type test rig.

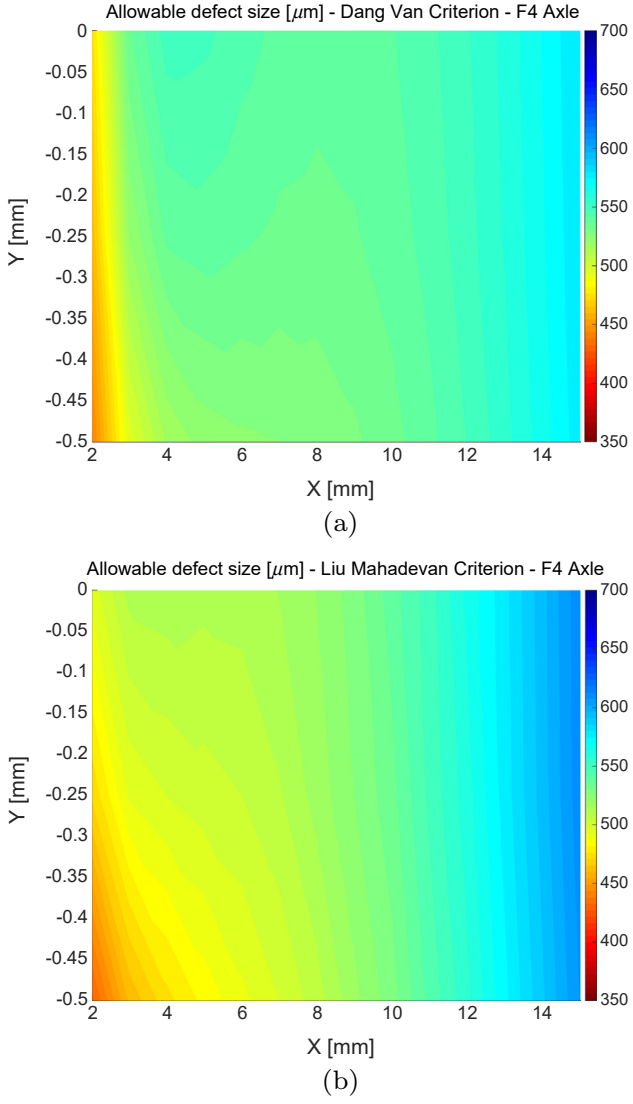

Fig. 11. Sub-surface critical defect size for F4 axle under run-out condition – Minden type test rig: (a) Dang van criterion, (b) Liu–Mahadevan criterion.

3.3. F4 axle

In Fig. 10, results showing the non-propagating crack size for F4 axle under two different loading conditions, failure and run-out, are presented. The region susceptible to crack propagation is found to be located at a distance of 4–8 mm away from transition edge. The Liu–Mahadevan criterion predicts a critical condition closer to the T-transition (Fig. 10).

When a nominal stress of 132 MPa (dashed line – failure condition in Fig. 10) is applied, allowable crack size is predicted to be 450 μm in length for the Dang Van criterion, while a size of 430 μm is the prediction made by the Liu–Mahadevan criterion. This limitation increases to a level of 500 μm for an applied stress of 120 MPa, which is the loading condition for run-out axles.

Applicability and prediction ability of the applied HCF criteria were checked by investigating the surface defects and the presence of non-propagating cracks. Micro and macro examinations of the contact along X direction were performed. Visual examination of the broken axles revealed presence of a major crack propagated through whole thickness located at a position 5 mm away from the transition edge (Fig. 2c). The run-out axle, tested at a nominal stress of 120 MPa, was sectioned in order to investigate presence of non-propagating cracks (Fig. 12). Measurements made on the run-out axle revealed the presence of material defects of 50–100 μms in depth with non propagating cracks in order of 100–150 μms in length. These results are in accordance with the limitation sets imposed by the application of the HCF criteria.

The critical plane orientation θ presented in Fig. 5b, independently from the applied nominal stress, is estimated to be equal to $\theta = 20^\circ$ for Dang Van criterion and $\theta = 40^\circ$ for the Liu–Mahadevan criterion. The estimation made by the Dang Van criterion is comparable with the angle measurements presented in Fig. 12.

In Fig. 11 subsurface analysis of the press-fit is presented for F4 axle. A slight sensitivity is observed as in the case of F1 axle.

The comparison between the two types of test rigs was made for failed F4 axles (Fig. 13). The predicted critical defect size was found to be approximately the same independent of the test rig used. However, considering the Vitry test rig, the predicted critical location for crack nucleation seems to be closer to the T-transition which is in contradiction with the experimental results, see Fig. 2b. A summary of the results for the acceptable defect size for F4 axles is presented in Table 3.

Finally, the comparison of the results with the inspection procedures presented in [7] was done. Hirakawa et. al. described an criterion of 150 μm defect size for the wheelset dismantled after 300000 km of service. In the present study, a critical defect size with 540 μm in length with an 20° inclination to the press-fit surface was determined. When projected to the depth axis ($d = c \sin\theta$) a 185 μm deep crack is achieved which is comparable in size with the acceptance criteria given.

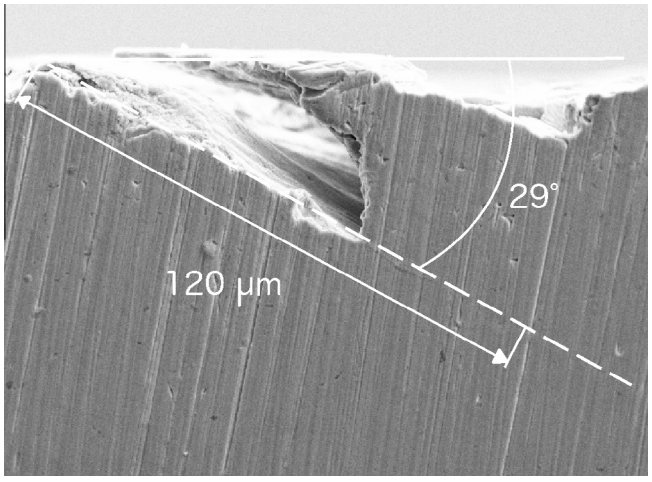

Fig. 12. Non propagating crack at run-out condition observed by the fractographic analysis for F4 axle.

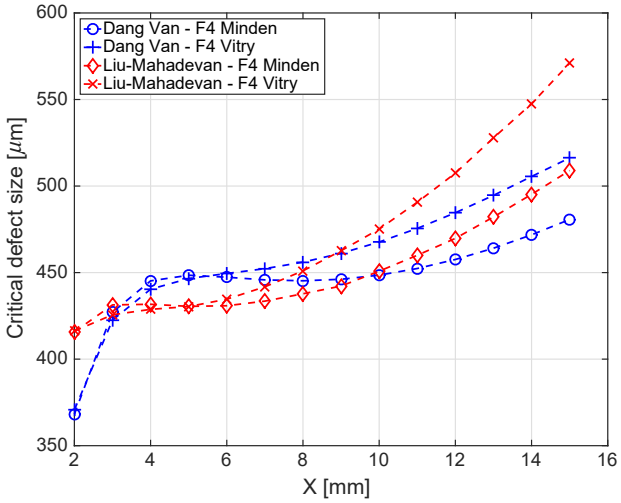

Fig. 13. Surface critical defect size for F4 axle at failure stress level – Minden vs Vitry type test rig.

4. Conclusion

In the present study an analytical model in order to study fretting fatigue is presented. The procedure is based on application of two different multiaxial fatigue criteria on the stress path present under the press-fit seat obtained by FE analysis. For each criterion, the equivalent stress defined by the applied multiaxial fatigue criterion is compared with the fatigue strength expressed by the El-Haddad correction for the given crack size. Allowable crack sizes at the onset of crack propagation, predicted by the multiaxial fatigue criteria, were defined as the limiting crack size for non-propagating cracks. Two different multiaxial fatigue criteria (Dang Van and Liu–Mahadevan) were applied on the FE results obtained by the analysis of stress path present along the press-fit contact and the results were compared with experimental results obtained in the Euraxles project. Considering the steep stress gradient encountered at the contact edge application of the presented method, which is based on the local stresses, has been limited to the point where the effect of stress singularity disappears. Starting from a point 2 mm away from the contact edge the selected multiaxial fatigue criteria were applied to the local stress state acquired by FE analysis.The examined region was selected in order to cover all the possible failure regions recorded by the post-test analysis of press-fit surface.

Both of the applied criteria provided reasonable estimates for possible sites of maximum fretting damage that are also consistent with the experimental results.Considering critical defect size, both criteria have provided results comparable to the crack size measurements obtained by fractographic analysis of tested F1 and F4 axles. Fractographic investigation of broken axles proved the presence of propagated cracks starting from multiple-site surface damage or from defects with a length of 350–400 μm. The predicted range is found to be in agreement with the permissible defect size predictions made by the applied criteria.

In addition, a great number of non-propagating cracks originating from surface defects were observed both on broken and run-

out axles. Size of non-propagating cracks are measured to reach 100–150 μms in length, which also justifies the critical size estimation made by the criteria.

The critical plane estimations made by Dang Van criterion were comparable with the experimental results. For this reason, modified Dang Van criterion can be concluded to be the most suitable approach for identification of susceptible regions.

In conclusion, the proposed method is able to establish a criterion for the acceptability of defect at press-fit in railway axles. The run-out conditions described by the mathematical method were verified by the failure analysis data collected from full-scale axle tests. The achieved acceptance criteria, which allows defects up to 500 μm in length and 200 μm in depth, is found to be compatible with the practical application presented in the literature.

Acknowledgement

Part of this research (analysis with modified Dang Van criterion) has been developed within the EU-FP7 Project EURAXLES "Minimizing the risk of fatigue failure of railway axles" – Grant agreement no: 265706.

G. Gurer participated in this research activity during the period he spent at PoliMi with a research assistant fellowship supported by the Department of Mechanical Engineering at Politecnico di Milano.

References

[1] Nesládek M, Španiel M, Jurenka J, Růžička J, Kuželka J. Fretting fatigue–experimental and numerical approaches. Int J Fatigue 2012;44:61–73.
[2] Waterhouse RB. Fretting corrosion. Pergamon Press; 1972.
[3] EN 13260 Railway applications. Wheelsets and bogies. Wheelsets. Product requirements; 2009.
[4] EN 13103 Railway applications. Wheelsets and bogies. Non powered axles. Design method; 2009.
[5] EN 13104 Railway applications. Wheelsets and bogies. Powered axles. Design method; 2009.
[6] EN 13261 Railway applications. Wheelsets and bogies. Axles. Product requirements; 2009.
[7] Hirakawa K, Toyama K, Kubota M. The analysis and prevention of failure in railway axles. Int J Fatigue 1998;20(2):135–44.
[8] Szolwinski MP, Farris TN. Mechanics of fretting fatigue crack formation. Wear 1996;198(1):93–107.
[9] Ekberg A. Fretting fatigue of railway axles—a review of predictive methods and an outline of a finite element model. Proc Inst Mech Eng F: J Rail Rapid Transit 2004;218(4):299–316.
[10] Navarro C, Muñoz S, Domínguez J. On the use of multiaxial fatigue criteria for fretting fatigue life assessment. Int J Fatigue 2008;30(1):32–44.
[11] Hills D, Nowell D, O'Connor J. On the mechanics of fretting fatigue. Wear 1988;125(1):129–46.
[12] Lykins CD, Mall S, Jain V. An evaluation of parameters for predicting fretting fatigue crack initiation. Int J Fatigue 2000;22(8):703–16.
[13] Hoeppner DW. Mechanisms of fretting fatigue and their impact on test methods development. ASTM Spec. Tech. Publ. 1992;1159:23.
[14] Dang Van K, Griveau B, Message O. On a new multiaxial fatigue limit criterion: theory and applications. In: Brown MW, Miller KJ, editors. EGF 3. London: Mechanical Engineering Publications; 1989. p. 479–96.
[15] Liu YM, Mahadevan S. Multiaxial high-cycle fatigue criterion and life prediction for metals. Int J Fatigue 2005;27(7):790–800. http://dx.doi.org/10.1016/j.ijfatigue.2005.01.003.
[16] Desimone H, Bernasconi A, Beretta S. On the application of Dang Van criterion to rolling contact fatigue. Wear 2006;260(4–5):567–72. http://dx.doi.org/10.1016/j.wear.2005.03.007.
[17] Foletti S, Beretta S, Tarantino MG. Multiaxial fatigue criteria versus experiments for small crack under rolling contact fatigue. Int J Fatigue 2014;58:181–92. http://dx.doi.org/10.1016/j.ijfatigue.2013.05.006.
[18] El Haddad M, Smith K, Topper T. Fatigue crack propagation of short cracks. J Eng Mater Technol 1979;101(1):42–6.
[19] Cervello S. Fatigue properties of railway axles: new results of full-scale specimens from EURAXLES project. Int J Fatigue 2016;86:2–12.
[20] Murakami Y. Metal fatigue: effects of small defects and nonmetallic inclusions: effects of small defects and nonmetallic inclusions. Elsevier; 2002.
[21] Araújo JA, Mamiya EN. The application of a mesoscopic scale approach in fretting fatigue. J Braz Soc Mech Sci Eng 2003;25(1):41–5.
[22] Sadeghi F, Jalalahmadi B, Slack TS, Raje N, Arakere NK. A review of rolling contact fatigue. J Tribol 2009;131(4):041403.
[23] Dang Van K. Macro–micro approach in high-cycle multiaxial fatigue. In: McDowell DL, Ellis R. (eds.), Advances in multiaxial fatigue, ASTM STP 1191; 1993. p. 120–30.
[24] Liu YM, Stratman B, Mahadevan S. Fatigue crack initiation life prediction of railroad wheels. Int J Fatigue 2006;28(7):747–56. http://dx.doi.org/10.1016/j.ijfatigue.2005.09.007.
[25] Beretta S, Murakami Y. SIF and threshold for small cracks at small notches under torsion. Fatigue Fract Eng Mater Struct 2000;23(2):97–104.
[26] Regazzi D, Filippini M, Beretta S. Small-scale fatigue tests on EA4T, Deliverable D3.2.1a, Tech. rep., EURAXLES European project; 2013.
[27] Beretta S, Carboni M. Material crack growth properties, Deliverable D7.1.3, Tech. rep., WIDEM European project; 2008.
[28] Accarino SA. Studio della resistenza a fretting di assili ferroviari in presenza di difetti [Master's thesis]. Politecnico di Milano; 2014.
[29] Landaberea Aea. Numerical analysis recommendations, Deliverable D2.4, Tech. rep., EURAXLES European project; 2013.
[30] Araujo J, Susmel L, Taylor D, Ferro J, Mamiya E. On the use of the theory of critical distances and the modified wöhler curve method to estimate fretting fatigue strength of cylindrical contacts. Int J Fatigue 2007;29(1):95–107.